Blind Self-Interference Analog Canceller with Differential Delay for Backscatter Communications

Koichi Nishikawa*, Shinsuke Ibi*, Takumi Takahashi†, and Hisato Iwai*
* Faculty of Science and Engineering, Doshisha University, 1-3 Tataramiyakodani, Kyotanabe, 610-0394, Japan
E-mail: ctwj0341@mail4.doshisha.ac.jp, {sibi, iwai}@mail.doshisha.ac.jp
† Graduate School of Engineering, Osaka University, Suita, Japan
E-mail: takahashi@comm.eng.osaka-u.ac.jp

***Abstract*—This paper demonstrates that the differential active self-interference canceller (DASIC), which does not require prior channel state information (CSI) of self-interference (SI), is effective in not only in-band full-duplex (IBFD) communications, but also backscatter communications. Unlike IBFD, backscatter communications have the characteristic that the desired signal is generated by nonlinear switching with rectangular pulse shape. Inspired by the characteristic, this paper proposes a method that enables cancellation in the analog domain by shortening the differential delay time of DASIC to a duration that can be implemented with a practical delay line. Additionally, focusing on the fact that the absolute value of the DASIC outputs remains constant regardless of the propagation delay time, an appropriate maximum *a-posteriori* probability (MAP) detector is designed for cases where the propagation delay time is unknown at the receiver. Finally, computer simulations confirm the efficacy of the proposed method by comparing the performance of MAP detectors when the propagation delay time is known and unknown, in terms of bit error rate (BER) performance.**

I. Introduction

With the rapid proliferation of Internet of Things (IoT) communications in recent years, there has been an increasing demand for low-power wireless communications to achieve a sustainable society. Bluetooth low energy (BLE) is a representative low-power communication method. However, even the BLE requires the generation of a carrier wave during transmission, which consumes tens of milliwatts of power. On the other hand, passive backscatter device (BD) performs energy harvesting (EH) from the received signals and convey information data by reflecting or absorbing the received signals. Therefore, BD does not need to generate a carrier wave, enabling ultra-low-power wireless communications, consuming only tens of microwatts, which has garnered significant attention [1]–[3].

Fig. 1 shows a typical configuration of backscatter communications from node B to node A. In this scenario, node B (BD) receives the signal sent from node A to node C, and sends its own information to node A by reflecting or absorbing the received signal. However, node A receives not only the desired signal from the BD but also its own transmission signal at a much higher power level as self-interference (SI). To address this issue for backscatter communications, the utilization of in-band full-duplex (IBFD) is a promising technique that allows simultaneous transmission and reception of signals within the same frequency band [4]–[6].

Typically, SI is suppressed using a combination of passive and active interference cancellers [7]–[9]. Passive cancellers enhance the path loss of the SI signal using specially designed antenna structures. On the other hand, active cancellers are divided into analog cancellers, which operate before the analog-to-digital converter (ADC), and digital cancellers, which work after the ADC [10]. In the active canceller, SI is mitigated as much as possible by subtracting a replica of the SI from the received signal. Ideally, in the active digital SI canceller (ASIC), the replica is generated flawlessly as the signal at the receiver is completely known. However, generating this replica requires periodic transmissions of orthogonal pilot signals to estimate channel state information (CSI). For instance, in wireless IoT scenarios where communication requests are random and intermittent, pilot signals must be transmitted even in the absence of communication requests, leading to inefficient wireless communication systems. To circumvent the increased communication overhead required for CSI acquisition, differential active SI canceller (DASIC) has been proposed, which eliminates the need for prior channel estimation of SI [11].

Additionally, when DASIC are implemented as a digital canceller, there is a problem where the desired signal cannot be extracted if the power level of the signal before the ADC is not within the ADC's dynamic range. However, to address the dynamic range issue by operating DASIC in the analog domain, a long delay line corresponding to the symbol period is required, which presents a significant challenge for implementations. In this paper, we propose a novel method that does not impair the effectiveness of DASIC operated in the analog domain, even with extremely short differential delays, by taking advantage of the characteristics of backscattered signals.

The contributions of this study are summarized as follows:

- After formulating the SI structure, we propose a method for applying DASIC to the analog domain by shortening the differential delay time.
- The probability density function (PDF) for the unknown propagation delay time from the BD is defined, and an appropriate maximum *a-posteriori* probability (MAP) detector that operates even when the delay time is unknown is designed.
- The efficacy of the proposed method is demonstrated by comparing the bit error rate (BER) performance for

known and unknown propagation delay times.

Notations: The symbol discrete time and the continuous time are represented by $[k]$ and (t), respectively. The real and complex number fields are denoted by $\mathbb{R}$ and $\mathbb{C}$, respectively. $(\cdot)^*$ represents complex conjugate. $\Re\{\cdot\}$ indicates the real part of complex numbers. The imaginary unit $\sqrt{-1}$ is denoted by j. $\mathbb{E}\{\cdot\}$ is the expected value.

II. System Model

A. Configuration of IBFD transceiver

Fig. 1 illustrates the configuration of the IBFD transceiver. On the transmitter side, information bits are modulated using Gaussian minimum shift keying (GMSK) and then converted into analog signals via a digital-to-analog converter (DAC). Analog signals are subsequently up-converted to radio frequency (RF) signals using an IQ mixer, filtered through a band-pass filter (BPF), and transmitted by an antenna. Conversely, on the receiver side, incoming signals are filtered through a BPF, down-converted using an IQ mixer, and then passed through a low-pass filter (LPF). The SI components present in analog signals are blindly canceled by the DASIC circuit. The DASIC outputs are then transformed into digital signals by ADC. Eventually, the information bits are detected by the demodulator based on the DASIC outputs.

B. Signal model of BLE

The RF signal $s_{\rm A}(t) \in \mathbb{R}$ transmitted from node A is represented as

$$s_{\rm A}(t) = \sqrt{2}\alpha\Re\{x_{\rm A}(t)\exp[{\rm j}\omega_{\rm c}t]\}, \tag{1}$$

where α is the amplitude of the RF signal, and $\omega_{\rm c}$ is the central angular frequency. The complex-valued baseband signal $x_{\rm A}(t) \in \mathbb{C}$ is represented by

$$x_{\rm A}(t) = \exp\left[{\rm j}\phi_{\rm A}(t)\right], \tag{2}$$

where $\phi_{\rm A}(t)$ is an information-bearing variable.

In this paper, assuming IoT communications between BLE devices, GMSK is used [12]. Denoting the symbol period by $T_{\rm s}$, within the interval $kT_{\rm s} \le t\ (= t' + kT_{\rm s}) < (k+1)T_{\rm s}$, the phase variable $\phi_{\rm A}(t)$ of GMSK can be expressed as [13], [14]

$$\phi_{\rm A}(t) = \pi \sum_{l=k-L+1}^{k} a_{\rm A}[l]q(t' + (k-l)T_{\rm s}) + \frac{\pi}{2}\sum_{l'=0}^{k-L} a_{\rm A}[l'], \tag{3}$$

where $a_{\rm A}[k] \in \{-1, 1\}$ is an information bit in a bipolar expression, and L is the memory size depending on the 3 dB bandwidth $B_{\rm G}$ of the Gaussian filter and the bandwidth-time product $B_{\rm G}T_{\rm s}$. The function $q(t)$ represents a phase pulse, which is defined by

$$q(t) = \int_{-\infty}^{t} g(\zeta)d\zeta, \tag{4}$$

under a constraint of

$$q(t) = \begin{cases} 0 & t \le 0, \\ 1/2 & t > LT_{\rm s}. \end{cases} \tag{5}$$

The function $g(\zeta)$ is a frequency pulse given by

$$g(\zeta) = \frac{1}{2T_{\rm s}}\left[Q\left(2\pi B_{\rm G}\frac{\zeta - T_{\rm s}/2}{\sqrt{\ln 2}}\right) - Q\left(2\pi B_{\rm G}\frac{\zeta + T_{\rm s}/2}{\sqrt{\ln 2}}\right)\right], \tag{6}$$

where $Q(\cdot)$ is the Q function.

C. Signal model of BD

Fig. 2 shows the configuration of the BD systems. The BD performs EH from the RF signal $s_{\rm A}(t)$ transmitted from node A to node C. Using a micro controller, the impedance of the antenna is switched, reflecting $s_{\rm A}(t)$ when the BD's information bit $a'_{\rm B}[k] = 1$, and absorbing it when $a'_{\rm B}[k] = 0$, where $a'_{\rm B}(t) \in \{0, 1\}$ is a pulse signal that can take values of 1 or 0. Consider the scenario in which node A receives a message from the BD. Let the propagation time for the signal transmitted from node A to be reflected by the BD and returned to the receiver of node A be τ $(0 \le \tau \le T_{\rm s})$. The received signal after passing through the LPF at node A is expressed as

$$r_{\rm A}(t) = h_{\rm AA}\alpha x_{\rm A}(t) + a'_{\rm B}(t)h_{\rm AB}\alpha x_{\rm A}(t-\tau) + z_{\rm A}(t), \tag{7}$$

where $h_{\rm AA}$ and $h_{\rm AB}$ represent the channel coefficients for the path A–A and A–B, respectively. $z_{\rm A}(t)$ denote a noise term that follows a complex Gaussian random process with a mean of 0 and a variance of $\beta = N_0/T_{\rm s}$, where N_0 is the noise power spectral density at one symbol interval. In (7), the first term represents the SI component, whereas the second term is the desired signal component.

III. DASIC for Backscatter Communications

A. Principle of DASIC

Let us consider operations of DASIC at node A when BD sends backscatter signal to node A. Fig. 3 shows the schematic of DASIC circuit with designated differential delay parameter d $(0 < d + \tau < T_{\rm s})$. The delay can be caused by using delay line, for example 10 ns[1]. With the known baseband signals $x_{\rm A}(t)$ and delayed $x_{\rm A}(t-d)$, the phase shift $\varphi_{\rm A}(t)$ used in the DASIC process is defined as

$$\varphi_{\rm A}(t) = \frac{x_{\rm A}(t)}{x_{\rm A}(t-d)}. \tag{8}$$

The DASIC output $\tilde{r}_{\rm A}(t)$ is obtained by subtracting $r_{\rm A}(t-d)$ multiplied by the phase shift $\varphi_{\rm A}(t)$ from $r_{\rm A}(t)$ as

$$\begin{aligned} \tilde{r}_{\rm A}(t) &= r_{\rm A}(t) - r_{\rm A}(t-d)\varphi_{\rm A}(t) \\ &= h_{\rm AB}\alpha\tilde{x}_{\rm A}(t-\tau) + \tilde{z}_{\rm A}(t), \end{aligned} \tag{9}$$

where the first term represents the desired signal component of the BD information, which is defined as

$$\begin{aligned} &\tilde{x}_{\rm A}(t-\tau) \\ &= a'_{\rm B}(t)x_{\rm A}(t-\tau) - a'_{\rm B}(t-d)x_{\rm A}(t-\tau-d)\varphi_{\rm A}(t), \end{aligned} \tag{10}$$

[1]This differs from the conventional DASIC of [11], which uses the symbol time $T_{\rm s}$ as the differential delay time for continuous GFSK signaling from node B to node A, making it difficult to implement with a delay line.

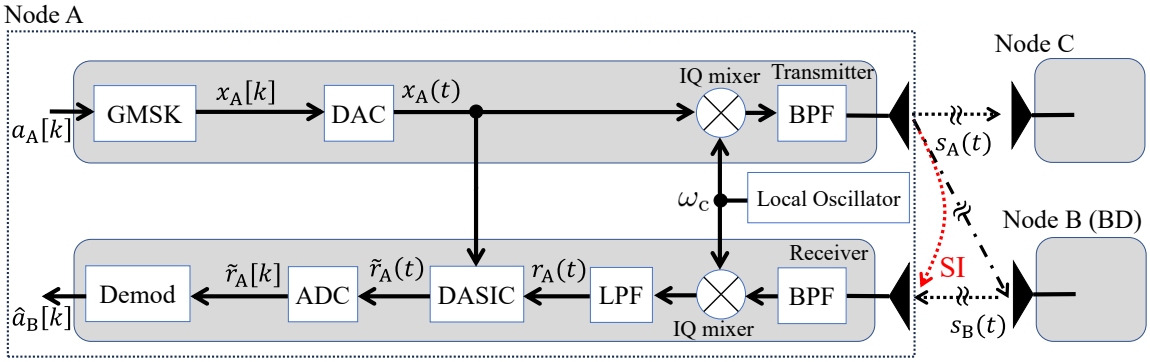

Fig. 1. Block diagram of DASIC-IBFD transceiver.

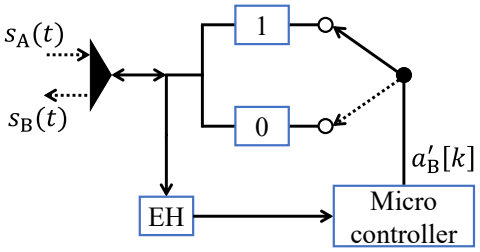

Fig. 2. Block diagram of BD.

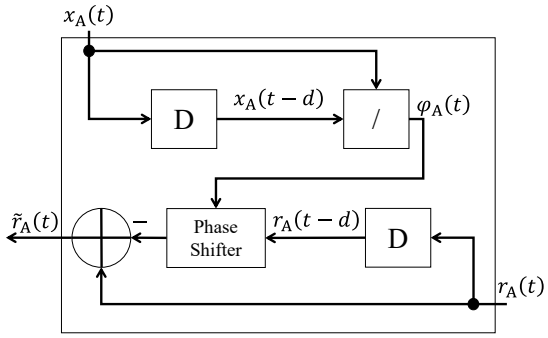

Fig. 3. Block diagram of DASIC process.

and the other term is noise component, which is expressed as

$$\tilde{z}_A(t) = z_A(t) - z_A(t-d)\varphi_A(t). \tag{11}$$

Note that nonlinear switching with rectangular pulse shape of BD signaling enables the avoidance of shrinking of the signal $\tilde{x}_A(t-\tau)$. If $a'_B(t) \approx a'_B(t-d)$ as in the conventional DASIC, it is obvious that (10) disappears. By utilizing the DASIC for BD systems, the SI component can be eliminated completely in (9) without shrinking $\tilde{x}_A(t-\tau)$.

Assuming the ideal sampling time at $t = kT_s + \Delta t$ that maximizes the eye aperture and $a'_B(t-d) = a'_B[k-1]$, the ADC of (9) yields

$$\tilde{r}_A[k] = h_{AB}\alpha\tilde{x}_A[k,\tau] + \tilde{z}_A[k], \tag{12}$$

where we have

$$\tilde{x}_A[k,\tau] = a'_B[k]x_A[k,\tau] - a'_B[k-1]x_A[k,\tau+d]\varphi_A[k], \tag{13}$$

$$\tilde{z}_A[k] = z_A[k] - z_A[k,d]\varphi_A[k], \tag{14}$$

and $x_A[k,\tau]$ represents the baseband signal sampled under the influence of the fractional propagation delay τ. Note that $\mathbb{E}\{|\tilde{z}_A[k]|^2\}$ is given by 2β because (14) has two noise variables.

When the memory size is $L = 3$ as an example, the constituent components $x_A[k,\tau]$, $x_A[k,\tau+d]$, and $\varphi_A[k]$ of $\tilde{x}_A[k,\tau]$ can be expressed as

$$x_A[k,\tau] = \exp\Big\{\mathrm{j}\omega_0(\tau)a_A[k] + \mathrm{j}\omega_1(\tau)a_A[k-1] + \mathrm{j}\omega_2(\tau)a_A[k-2] + \mathrm{j}\sigma_A[k-3]\Big\}, \tag{15}$$

$$x_A[k,\tau+d] = \exp\Big\{\mathrm{j}\omega_0(\tau+d)a_A[k] + \mathrm{j}\omega_1(\tau+d)a_A[k] + \mathrm{j}\omega_2(\tau+d)a_A[k-2] + \mathrm{j}\sigma_A[k-3]\Big\}, \tag{16}$$

$$\varphi_A[k] = \exp\Big\{\mathrm{j}(\omega_0(0) - \omega_0(d))a_A[k] + \mathrm{j}(\omega_1(0) - \omega_1(d))a_A[k-1] + \mathrm{j}(\omega_2(0) - \omega_2(d))a_A[k-2]\Big\}, \tag{17}$$

where we have

$$\omega_l(\tau) = \pi q(\Delta t - \tau + lT_s), (l \in \{0,1,2\}), \tag{18}$$

$$\sigma_A[k] = \frac{\pi}{2}\sum_{l=0}^{k} a_A[l]. \tag{19}$$

B. Threshold for simple successive hard decision

Hereafter, to simplify the discussion, the case of MSK ($B_G T_s = \infty$) is considered. In this case, sampling at the timing $t' = \Delta t$ when the eye aperture is maximized results in

$$\omega_0(\tau) = 0,\ \omega_1(\tau) = \frac{T_s - \tau}{2T_s}\pi,\ \omega_2(\tau) = \frac{\pi}{2}. \tag{20}$$

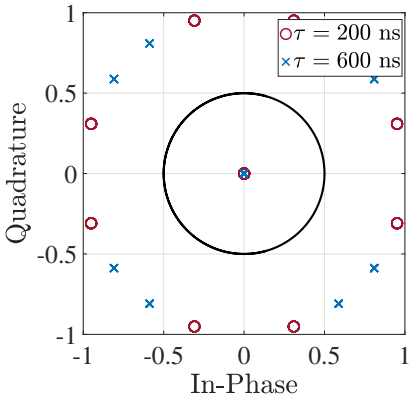

Fig. 4. Constellation of $\tilde{r}_{\rm A}[k]$: $h_{\rm AB}\alpha = 1, \tilde{z}_{\rm A}[k] = 0$.

Using (20), (15)∼(17) can be rewritten as

$$x_{\rm A}[k,\tau] = \exp\left\{{\rm j}\frac{T_{\rm s}-\tau}{2T_{\rm s}}\pi a_{\rm A}[k-1] + {\rm j}\sigma_{\rm A}[k-2]\right\}, \quad (21)$$

$$x_{\rm A}[k,\tau+d] = \exp\left\{{\rm j}\frac{T_{\rm s}-\tau-d}{2T_{\rm s}}\pi a_{\rm A}[k-1] + {\rm j}\sigma_{\rm A}[k-2]\right\}, \quad (22)$$

$$\varphi_{\rm A}[k] = \exp\left\{{\rm j}\frac{d}{2T_{\rm s}}\pi a_{\rm A}[k-1]\right\}. \quad (23)$$

By defining $\tilde{a}_{\rm B}[k] = a'_{\rm B}[k] - a'_{\rm B}[k-1] \ \in \{0, \pm 1\}$, (13) can be interpreted as

$$\begin{aligned}\tilde{x}_{\rm A}[k,\tau] &= a'_{\rm B}[k]\exp\left\{{\rm j}\frac{T_{\rm s}-\tau}{2T_{\rm s}}\pi a_{\rm A}[k-1] + {\rm j}\sigma_{\rm A}[k-2]\right\} \\ &\quad - a'_{\rm B}[k-1]\exp\left\{{\rm j}\frac{T_{\rm s}-\tau-d}{2T_{\rm s}}\pi a_{\rm A}[k-1]\right. \\ &\qquad \left. + {\rm j}\sigma_{\rm A}[k-2] + {\rm j}\frac{d}{2T_{\rm s}}\pi a_{\rm A}[k-1]\right\} \\ &= (a'_{\rm B}[k] - a'_{\rm B}[k-1]) \\ &\quad \cdot \exp\left\{{\rm j}\frac{T_{\rm s}-\tau}{2T_{\rm s}}\pi a_{\rm A}[k-1] + {\rm j}\sigma_{\rm A}[k-2]\right\} \\ &= \tilde{a}_{\rm B}[k]x_{\rm A}[k,\tau] \quad (24) \\ &= \begin{cases} \pm x_{\rm A}[k,\tau] & (\tilde{a}_{\rm B}[k] \neq 0), \\ 0 & (\tilde{a}_{\rm B}[k] = 0). \end{cases}\end{aligned}$$

As shown in Fig. 4, because $|\tilde{x}_{\rm A}[k,\tau]| = 1$ does not depend on τ, if $a'_{\rm B}[k-1]$ is known by successive detection, simple hard decision is possible even when τ is unknown. Therefore, the threshold value for hard decision is set to $|h_{\rm AB}|\alpha/2$, and decisions are successively made from $k = 1$ as

$$\hat{a}'_{\rm B}[k] = \begin{cases} \hat{a}'_{\rm B}[k-1] & (|\tilde{r}_{\rm A}[k]| \leq |h_{\rm AB}|\alpha/2), \\ -\hat{a}'_{\rm B}[k-1] + 1 & (|\tilde{r}_{\rm A}[k]| > |h_{\rm AB}|\alpha/2). \end{cases} \quad (25)$$

Thus, unlike IBFD of [11], signal detection is possible in backscatter communications even with an extremely short differential delay d.

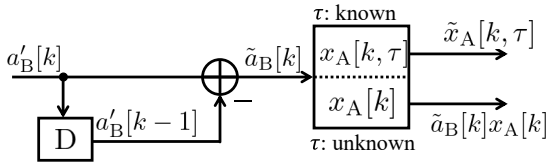

Fig. 5. Structure of IIR filter in DASIC when τ is known and unknown.

C. MAP detector with knowledge on τ

In the case of successive hard detection, the problem is that performance degrades due to the propagation of decision errors. Therefore, let us investigate MAP detector, which can achieve optimal performance according to probabilistic theory to deal with the error propagation problem. Within the MAP framework, the log-likelihood ratio (LLR) is defined as

$$\lambda_{\rm B}[k] = \ln\frac{\Pr[a'_{\rm B}[k]=1 \mid \{\tilde{r}_{\rm A}[k]\}]}{\Pr[a'_{\rm B}[k]=0 \mid \{\tilde{r}_{\rm A}[k]\}]}, \quad (26)$$

where $\{\tilde{r}_{\rm A}[k]\}$ denotes a sequence of $\tilde{r}_{\rm A}[k]$. Assuming that τ is known, the structure of the infinite impulse response (IIR) filter for $\tilde{x}_{\rm A}[k,\tau]$ generation is illustrated in Fig. 5 with memory size of 1. In this case, the number of states in the trellis diagram is two because $a'_{\rm B}[k-1]$ has zero or one. Therefore, the complexity is not so high.

Based on the trellis diagram of the IIR filter, the LLR can be calculated using the BCJR algorithm [15], without requiring a significant computational burden. The transition (joint) probability required for the BCJR process is given by

$$\Pr[\tilde{a}_{\rm B}[k] \mid \tilde{r}_{\rm A}[k]] \propto \exp\left\{-\frac{|\tilde{r}_{\rm A}[k] - h_{\rm AB}\alpha\tilde{a}_{\rm B}[k]x_{\rm A}[k,\tau]|^2}{2\beta}\right\}. \quad (27)$$

D. MAP detector without knowledge on τ

In the previous subsection, the MAP detector is designed by assuming that the propagation delay time τ is known. However, if node A or BD is moving, it is difficult to stably estimate τ, making τ unknown. Therefore, in this subsection, a MAP detector capable of detection even when τ is unknown is designed.

Using (21) and (24), $\tilde{x}_{\rm A}[k,\tau]$ can be rewritten as

$$\tilde{x}_{\rm A}[k,\tau] = \tilde{a}_{\rm B}[k]x_{\rm A}[k]\exp\left\{-{\rm j}\theta_\tau a_{\rm A}[k-1]\right\}, \quad (28)$$

where we have $\theta_\tau = \pi\tau/2T_{\rm s}$ $(0 < \theta_\tau < \pi/2)$. Then assuming that θ_τ is uniformly distributed, the PDF of $\tilde{r}_{\rm A}[k]$ when τ is

unknown is given by

$$
\begin{aligned}
&p(\tilde{r}_{\mathrm{A}}[k] \mid \tilde{a}_{\mathrm{B}}[k], h_{\mathrm{AB}}, x_{\mathrm{A}}[k]) \\
&= \int_0^{\frac{\pi}{2}} p(\theta_\tau) p(\tilde{r}_{\mathrm{A}}[k] \mid \tilde{a}_{\mathrm{B}}[k], h_{\mathrm{AB}}, x_{\mathrm{A}}[k,\tau]) d\theta_\tau \\
&= \int_0^{\frac{\pi}{2}} \frac{2}{\pi} \cdot \frac{1}{2\pi\beta} \exp\left\{ -\frac{|\tilde{r}_{\mathrm{A}}[k] - h_{\mathrm{AB}}\alpha\tilde{a}_{\mathrm{B}}[k] x_{\mathrm{A}}[k,\tau]|^2}{2\beta} \right\} d\theta_\tau \\
&= \frac{1}{\pi^2\beta} \exp\left[-\frac{1}{2\beta} \left\{ |\tilde{r}_{\mathrm{A}}[k]|^2 + |h_{\mathrm{AB}}\alpha\tilde{a}_{\mathrm{B}}[k]|^2 \right\} \right] \\
&\quad \cdot \int_0^{\frac{\pi}{2}} \exp\left[\frac{1}{\beta} \Re\left\{ \tilde{r}_{\mathrm{A}}^*[k] h_{\mathrm{AB}} \alpha x_{\mathrm{A}}[k,\tau] \tilde{a}_{\mathrm{B}}[k] \right\} \right] d\theta_\tau. \qquad (29)
\end{aligned}
$$

Then, using (28), the component of (29) can be rewritten as

$$
\begin{aligned}
&\Re\left\{ \tilde{r}_{\mathrm{A}}^*[k] h_{\mathrm{AB}} \alpha x_{\mathrm{A}}[k,\tau] \tilde{a}_{\mathrm{B}}[k] \right\} \\
&\quad = \Re\left\{ |\tilde{r}_{\mathrm{A}}^*[k] h_{\mathrm{AB}} \alpha \tilde{a}_{\mathrm{B}}[k]| \exp\left[\mathrm{j}(-\theta_\tau a_{\mathrm{A}}[k-1] + \psi) \right] \right\} \\
&\quad = |\tilde{r}_{\mathrm{A}}^*[k] h_{\mathrm{AB}} \alpha \tilde{a}_{\mathrm{B}}[k]| \cos(-\theta_\tau a_{\mathrm{A}}[k-1] + \psi), \qquad (30)
\end{aligned}
$$

where we have ψ $(-\pi < \psi \leq \pi)$ as

$$
\psi = \arg\left\{ \tilde{r}^*[k] h_{\mathrm{AB}} \alpha \tilde{a}_{\mathrm{B}}[k] x_{\mathrm{A}}[k] \right\}. \qquad (31)
$$

Finally, applying (30) to (29) yields

$$
\begin{aligned}
&p(\tilde{r}_{\mathrm{A}}[k] \mid \tilde{a}_{\mathrm{B}}[k], h_{\mathrm{AB}}, x_{\mathrm{A}}[k]) \\
&\qquad \propto \xi(\psi) \exp\left\{ -\frac{|h_{\mathrm{AB}}\alpha\tilde{a}_{\mathrm{B}}[k]|^2}{2\beta} \right\}, \qquad (32)
\end{aligned}
$$

where we have

$$
\begin{aligned}
&\xi(\psi) = a_{\mathrm{A}}[k-1] \\
&\quad \cdot \int_{-\frac{\pi}{2} a_{\mathrm{A}}[k-1] + \psi}^{\psi} \exp\left[\frac{|\tilde{r}_{\mathrm{A}}^*[k] h_{\mathrm{AB}} \alpha \tilde{a}_{\mathrm{B}}[k]|}{\beta} \cos\theta'_\tau \right] d\theta'_\tau, \qquad (33)
\end{aligned}
$$

with $\theta'_\tau = -\theta_\tau a_{\mathrm{A}}[k-1] + \psi$.

The transition (joint) probability for BCJR is given as

$$
\Pr[\tilde{a}_{\mathrm{B}}[k] \mid \tilde{r}_{\mathrm{A}}[k]] \propto \xi(\psi) \exp\left\{ -\frac{|h_{\mathrm{AB}}\alpha\tilde{a}_{\mathrm{B}}[k]|^2}{2\beta} \right\}. \qquad (34)
$$

In (34), $\xi(\psi)$ is computed by piece-wise quadrature method.

IV. Simulation Results

Computer simulations were conducted to validate the efficacy of the proposed method. The modulation scheme is GMSK ($B_{\mathrm{G}}T_{\mathrm{s}} = 0.5, L = 3$), assuming that BLE is used. Each information block is composed of 64 bits. The symbol period and the differential delay are $T_{\mathrm{s}} = 1$ μs and $d = 10$ ns, respectively. The channel coefficient h_{AB} is assumed to be known at the receiver, whereas h_{AA} is unknown. Let η be signal-to-interference power ratio (SIR), which is defined as

$$
\eta = 10 \log_{10} \frac{|h_{\mathrm{AB}}|^2}{|h_{\mathrm{AA}}|^2} \quad [\mathrm{dB}]. \qquad (35)
$$

Fig. 6 shows the BER versus $|h_{\mathrm{AB}}|^2 E_{\mathrm{s}}/N_0$ performance. Although the channels follow Rayleigh fading, the horizontal axis represents the instantaneous $|h_{\mathrm{AB}}|^2 E_{\mathrm{s}}/N_0$ rather than the average. As a result, it is equivalent to a channel influenced by phase rotation without amplitude fluctuations.

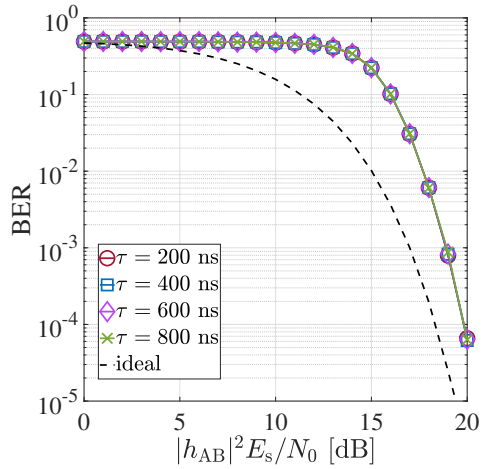

(a) Successive hard detection.

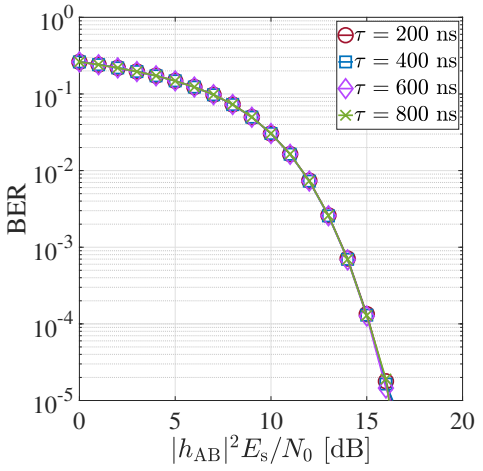

(b) MAP decision: τ is known.

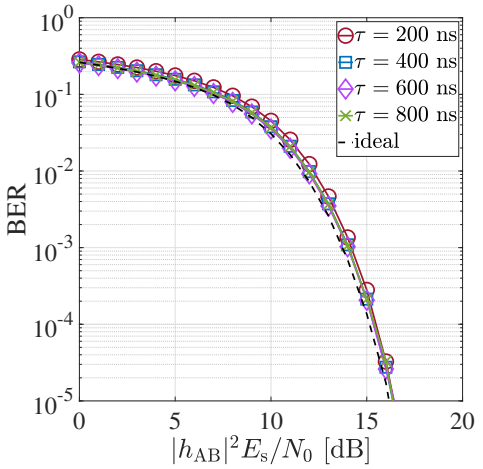

(c) MAP decision: τ is unknown.

Fig. 6. BER performance of DASIC: $\eta = -50$ dB.

Fig. 6(a) shows the detection capability of the successive hard decision. The "ideal" curve represents the performance assuming that all successive estimates are ideally correct ($\hat{a}'_{\mathrm{B}}[k-1] = a'_{\mathrm{B}}[k-1]$). The performance remains BER ≥ 0.34 until $|h_{\mathrm{AB}}|^2 E_{\mathrm{s}}/N_0 = 14$ dB, but starts to decrease at $|h_{\mathrm{AB}}|^2 E_{\mathrm{s}}/N_0 = 15$ dB, reaching BER $< 10^{-4}$

at $|h_{\rm AB}|^2 E_{\rm s}/N_0 = 19.8$ dB, whereas "ideal" achieves BER $< 10^{-4}$ at $|h_{\rm AB}|^2 E_{\rm s}/N_0 = 18.3$ dB. This degradation is due to error propagation during successive detection. However, in the case of hard decision, the performance is consistent regardless of the propagation delay time τ, indicating that signal detection is possible even when τ is unknown.

Fig. 6(b) shows the performance of the MAP detection using (27) when τ is known. Because MAP detector is designed assuming τ is known, the performance is consistent regardless of τ. As expected, the performance degradation caused by successive hard decision is improved. Remarkably, the required $|h_{\rm AB}|^2 E_{\rm s}/N_0$ to satisfy BER $< 10^{-4}$ is 15.1 dB, improving the performance in hard decision by 4.7 dB. However, such a good performance, using (27), cannot be achieved unless τ is known.

On the other hand, Fig. 6(c) shows the performance of MAP detection using (34) when τ is unknown. The "ideal" curve represents the performance in Fig. 6(b) when τ is known. The required $|h_{\rm AB}|^2 E_{\rm s}/N_0$s to satisfy BER $< 10^{-2}$ at $\tau = 200$, $\tau = 400$, $\tau = 600$ and $\tau = 800$ ns are 12.2 dB, 12.0 dB, 12.0 dB, 11.9 dB, respectively, exhibiting slightly different performance depending on τ. This is because (34) is designed assuming MSK, and the Euclidean distance for $\tilde{a}_{\rm B}[k] = \pm 1$ varies depending on τ. Remarkably, BER $\leq 10^{-5}$ is achieved at $|h_{\rm AB}|^2 E_{\rm s}/N_0 = 16.4$ dB compared with $|h_{\rm AB}|^2 E_{\rm s}/N_0 = 16.2$ dB in the "ideal" case, indicating that while the performance degrades when τ is unknown, the degradation is limited to within 0.2 dB. Therefore, it can be concluded that MAP detection when τ is unknown is the most effective method for practical environments.

V. Conclusion

To address the problem of SI cancellation being required in backscatter communications just as in IBFD, this paper demonstrated that DASIC, which has been effective in IBFD, is also effective in backscatter communications. Additionally, by leveraging the characteristics of backscatter communications, where the desired signal is the delayed path of the terminal itself, the differential delay is shortened, enabling the application of DASIC in the analog domain. Furthermore, a MAP detector that operates even when τ is unknown is designed. The results show only a 0.2 dB degradation compared to the case where τ is known, concluding that this is the most practical approach.

Acknowledgment

A part of this work was supported by JSPS KAKENHI Grant Number JP23K20935 and JP23K22754, Japan.

References

[1] M. A. Alim, S. Saruwatari, and T. Watanabe, "Backscatter mac protocol for future internet of things networks," in *2017 IEEE 13th International Conference on Wireless and Mobile Computing, Networking and Communications (WiMob)*, 2017, pp. 1–7.

[2] M. Zhang, J. Zhao, S. Chen, and W. Gong, "Reliable backscatter with commodity BLE," in *IEEE INFOCOM 2020 - IEEE Conference on Computer Communications*, 2020, pp. 1291–1299.

[3] B. Kellogg, A. Parks, S. Gollakota, J. R. Smith, and D. Wetherall, "Wi-fi backscatter: Internet connectivity for RF-powered devices," *SIGCOMM Comput. Commun. Rev.*, vol. 44, no. 4, pp. 607–618, Aug. 2014.

[4] D. Bharadia, E. McMilin, and S. Katti, "Full duplex radios," *ACM SIGCOMM 2013*, pp. 375–386, Aug. 2013.

[5] Z. Zhang, K. Long, A. V. Vasilakos, and L. Hanzo, "Full-duplex wireless communications: Challenges, solutions and future research directions," *in Proc.IEEE*, vol. 104, pp. 1369–1409, Jul. 2016.

[6] K. E. Kolodziej, B. T. Perry, and J. S. Herd, "In-band full-duplex technology: Techniques and systems survey," *IEEE Transactions on Microwave Theory and Techniques*, vol. 67, no. 7, pp. 3025–3041, 2019.

[7] Z. Zhang, X. Chai, K. Long, A. V. Vasilakos, and L. Hanzo, "Full duplex techniques for 5G networks: Self-interference cancellation, protocol design, and relay selection," *IEEE Communications Magazine*, vol. 53, no. 5, pp. 128–137, 2015.

[8] A. Sahai, G. Patel, C. Dick, and A. Sabharwal, "On the impact of phase noise on active cancelation in wireless full-duplex," *IEEE Trans. Veh. Commun.*, vol. 62, no. 9, pp. 4494–4510, Nov. 2013.

[9] E. Everett, A. Sahai, and A. Sabharwal, "Passive self-interference suppression for full-duplex infrastructure nodes," *IEEE Trans. Wireless Commun.*, vol. 13, no. 2, pp. 680–694, Feb. 2014.

[10] A. Sabharwal, P. Schniter, D. Guo, D. W. Bliss, S. Rangarajan, and R. Wichman, "In-band full-duplex wireless: Challenges and opportunities," *IEEE Journal on Selected Areas in Communications*, vol. 32, no. 9, pp. 1637–1652, 2014.

[11] S. Ibi, T. Takahashi, and H. Iwai, "Differential active self-interference cancellation for asynchronous in-band full-duplex GFSK," *IEICE Trans. Commun.*, vol. E107-B, no. 8, pp. 552–563, Aug. 2024.

[12] Core Specification Working Group, *Bluetooth core specification*, 2021.

[13] R. H.-H. Yang, C.-K. Lee, and S.-J. Chern, "Performance improvement of the catastrophic CPM scheme with new split-merged MNSED," *IEICE Trans. Commun.*, vol. E102-B, no. 11, pp. 2091–2103, Nov. 2019.

[14] B. E. Rimoldi, "A decomposition approach to CPM," *IEEE Trans. Inf. Theory.*, vol. 34, no. 2, pp. 260–270, Mar. 1988.

[15] L. Hanzo, T. Liew, and B. Yeap, *Turbo Coding, Turbo Equalisation and Space-Time Coding*. New York: Wiley, 2002.